

Comparison of X-ray diffraction measurement of residual elastic strains: monochromatic beam and image plate versus white beam energy-dispersive analysis

W J J Vorster^{1*}, S Y Zhang¹, M Golshan², D Laundy², D Dini¹, and A M Korsunsky¹

¹Department of Engineering Science, University of Oxford, Oxford, UK

²CCLRC Daresbury Laboratory, Warrington, Cheshire, UK

The manuscript was received on 12 May 2006 and was accepted after revision for publication on 11 September 2006.

DOI: 10.1243/03093247JSA238

Abstract: This paper presents the results of synchrotron X-ray diffraction measurement of residual elastic strains in a bent magnesium alloy bar using two different techniques. In the first technique the sample was scanned transversely to a monochromatic X-ray beam. The scattered X-rays were recorded on a phosphoric image plate that was translated at a proportional speed but in the opposite direction to the sample. This enabled the creation of a two-dimensional recording of one-dimensional diffraction patterns. In the second technique a white X-ray beam is used in combination with an energy-discriminating detector mounted at a fixed angle to record similar patterns at each gauge volume position within the sample.

The motivation for comparing the results of two measurement techniques is to establish whether the same accuracy in a diffraction strain evaluation can be achieved. It was found that the translating image plate arrangement requires a certain amount of care in calibration and interpretation, but provides a quick and efficient method that can be competitive with the white beam energy-dispersive mode which is known to deliver a fast diffraction capability.

Keywords: X-ray diffraction, image plate, energy dispersive, residual elastic strain, Mg alloy

1 INTRODUCTION

In the last decade strain scanning using synchrotron radiation has become an important tool, helping to characterize residual stress states in engineering structures [1] in order to improve the manufacturing processes by reducing distortion and increasing the durability of key components. X-ray diffraction scanning is a high-resolution non-destructive technique that can provide information on stress and strain fields within engineering components. Diffraction techniques most commonly used to measure strain include neutron diffraction, conventional (laboratory) X-ray, and synchrotron X-ray diffraction. The unique non-destructive nature

of these measurement techniques is particularly beneficial in the context of engineering design since it allows the evaluation of a variety of structural and deformation parameters inside real components without material removal, or at worst with minimal interference. X-ray diffractometry has great flexibility in allowing measurements to be made on fine-grained powders and polycrystalline aggregates, as well as individual grains or single crystals, and also on amorphous materials and glasses.

The measurements described in this paper were made at the Synchrotron Radiation Source (SRS) station 16.3 in Daresbury, UK. The source is a 6 T superconducting wavelength shifter, delivering X-rays ranging from 5 to 80 keV [1]. Synchrotron X-ray beams are preferred for diffraction experiments since they offer high photon flux and excellent beam parallelism, offering the ability to achieve high spatial resolution and peak shape definition with

*Corresponding author: Department of Engineering Science, University of Oxford, 13 Parks Road, Oxford, OX1 3PJ, UK. email: willem.vorster@eng.ox.ac.uk

short counting times. High-energy photons possess greater penetration depth, allowing data collection from sampling volumes embedded within the bulk of the material, rather than thin surface layers as in the case of conventional laboratory X-rays.

Synchrotron high-energy X-ray diffraction has undergone rapid development over the last decade, primarily as far as the experimental techniques are concerned. Strain scanning experiments have been performed at the European Synchrotron Radiation Facility (ESRF), Daresbury, and many other synchrotron facilities using the monochromatic mode [2] and white beam mode [1]. Interpretation of diffraction patterns has been carried out using various approaches, notably those utilizing whole pattern refinement procedures [3–5]. Simultaneous interpretation of multiple peaks offers great advantages for estimating the macroscopic average elastic strain that is often the purpose of the experiment. Errors in strain measurements using X-ray diffraction of the order of 10^{-4} or better can be readily achieved.

Relatively little progress has been made in the field of mechanics interpretation of the measured residual elastic strains. A significant aspect of high-energy X-ray diffraction measurement is the fact that the Bragg scattering angle is necessarily found to be small, and hence the sampling volumes become elongated in the direction of the incident beam. It is therefore impossible to measure the diffraction strain in directions close to the incident beam, and it is also impossible to achieve very good spatial resolution in that direction. In practice this often means that, even if the specimen is rotated in the beam to allow the measurement of different strain components, the low spatial resolution along the beam must be overcome by some analysis tool. A novel family of variational approaches has been proposed for this purpose [1, 6].

In the present study two different methods were used to collect diffraction patterns from a plastically bent magnesium alloy bar (Fig. 1). Magnesium alloys are potentially useful as structural material owing to their high strength–weight ratio, conductivity, and recyclability compared with other alloys [7]. Magnesium has prompted much interest in the automobile, computer, consumer electronic, and sports industries. However, its use is limited owing to its low corrosion resistance in certain environments [8].

The primary purpose of the experiments was to extract the profile of the longitudinal, or directed along the y direction shown in Fig. 2, macroscopic average residual elastic strain. The first method involved the use of a monochromatic beam obtained with the help of a Laue monochromator made from a

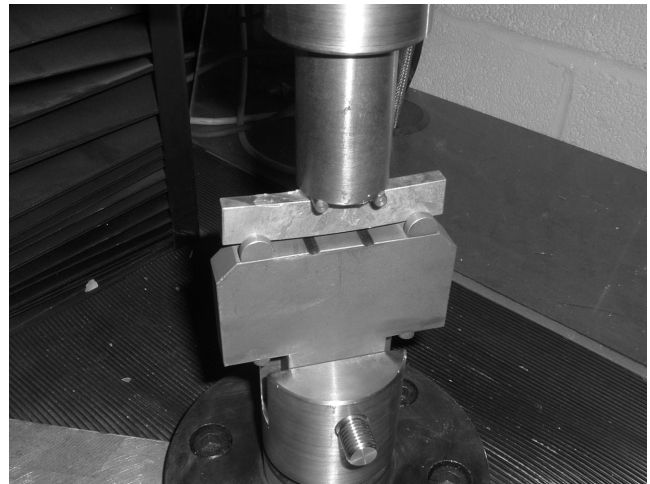


Fig. 1 Loading device

single sagittally bent silicon crystal and of a phosphor image plate (IP) mounted on a translation stage travelling transversely with respect to the incident beam. The second set-up made use of the white (polychromatic) beam obtained from the insertion device, in combination with a liquid nitrogen cooled Ge detector (Canberra Model 8706 ADC), which provided energy discrimination to better than 300 eV FWHM (full-width at half-maximum). The white beam mode provides very high counting efficiency since a much broader bandwidth is used to collect multiple reflections simultaneously. However, diffraction peak shape definition in particular is limited to the resolution of the energy-dispersive (ED) detector used [1]. Nevertheless, the photon counts are potentially several orders of magnitude greater than those for monochromatic beams, so that, with appropriate analyses using multiple peak data or whole pattern refinement algorithms, an accurate and fast determination of lattice spacings is possible.

Narrow bandwidths of photon energy or wavelengths are required for the monochromatic beam mode, with $\Delta E_\lambda/E_\lambda$ usually in the range between 10^{-3} and 10^{-4} . Monochromatic X-ray beam diffraction allows accurate determination of diffraction peak intensities, shapes, and positions. These diffraction patterns are either recorded using a detector scanning over a range of the diffraction scattering angle 2θ , or with a position-sensitive detector capable of registering the distribution of photon flux along a line or over a two-dimensional surface. Compared with the ED mode, this method requires significantly longer counting times to collect the data from comparable sections of the diffraction pattern, owing to the reduced photon flux and because of the need for detector scanning. In the experiments under

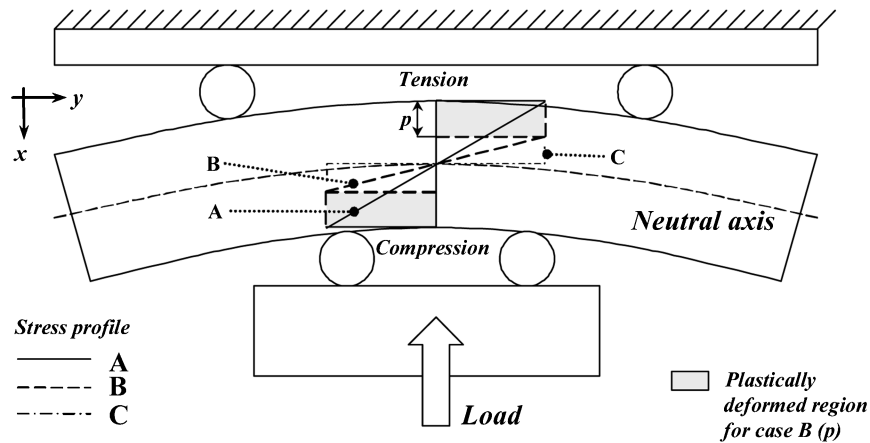


Fig. 2 Illustration of plastic deformation of the bar in four-point bending

discussion, the recording of the scattered monochromatic beam pattern was made using a phosphor IP rather than a scanning detector. IP technology is well known for providing a small pixel size and a large dynamic range, which are superior compared with most digital readout techniques. Furthermore, the two-dimensional surface of the IP can be used in combination with a defining slit (say, vertical) and a translation mount (say, horizontal) in order to collect multiple diffraction line patterns on to a single image.

The present paper discusses how the combination of monochromatic beam with a translating IP can provide a competitive method for fast diffraction data measurement, achieving data collection rates comparable with those using the white beam mode. Furthermore, the higher resolution of the IP results in improved accuracy compared with those from a scanning detector. Some difficulties of implementation must be overcome in order to obtain the best data using this method, particularly those associated with IP orientation and accounting for distortions.

The benefits of multiple-peak diffraction analysis for material deformation studies have been discussed elsewhere [6] and above. However, the focus of the present paper will primarily be placed on the experimental techniques used for mapping the residual stress distribution within the bent magnesium alloy bar, rather than on the modelling of microstructural aspects of materials engineering. The primary objectives of the paper are therefore (a) to collect and interpret residual elastic strain using a monochromatic X-ray beam and a translated phosphor IP, (b) to compare the strain profiles obtained from the former method with those found using white beam experiments, and finally (c) to assess the accuracy of the proposed methodology and discuss the range of possible applications.

2 EXPERIMENTAL PROCEDURE

The sample used for the experiment was made from die-cast magnesium alloy AM60B-F (casting temperature 650 °C). The composition of the alloy given in weight per cent is approximately 94%Mg, 5.5%Al, and small amounts of additional alloying elements Cu, Fe, Mn, Ni, Zn, and Si. Table 1 summarizes the physical and mechanical properties of this magnesium alloy. The sample was made into the form of a bar of dimensions 80 mm (length) by 15 mm (height) by 6.35 mm (thickness).

The bar of magnesium alloy AM60B-F was bent by applying a bending moment M_z using a universal testing machine within a four-point bending attachment, as shown in Fig. 1. The lines labelled A, B, and C in Fig. 2 correspond to the longitudinal elastic strain (and hence longitudinal stress) under progressively increasing applied bending moment for the case of non-work-hardening material (elastic-ideally plastic). When the applied moment reaches the critical value required for yielding, the stress (and elastic strain) distribution across the bar is linear (line A). When the applied moment is increased (line B), the material undergoes progressive plastic yielding from the surface. The total strain remains linear across the

Table 1 Material properties

Properties	Value	Comment
Density (g/cm ³)	1.8	
Hardness, Brinell	65	500 kg load, 10 mm ball
Tensile strength, ultimate (MPa)	241	
Tensile strength, yield (MPa)	131	
Elongation at break (%)	13	In 50 mm
Modulus of elasticity (GPa)	45	
Compressive yield strength (MPa)	131	
Poisson's ratio	0.35	

beam, but a proportion of it is now accommodated plastically. If the moment is increased further (line C) the plastic zone also grows by expanding towards the centre of the bar.

If the material undergoes work hardening during deformation then its response to inelastic bending and the resulting residual stress state are somewhat more complex [9], as illustrated in Fig. 3. Within the framework of beam-bending approximation used in this study the macroscopic average elastic strain and residual longitudinal stress may be thought to be proportional to each other, with Young's modulus serving as the constant of pro-

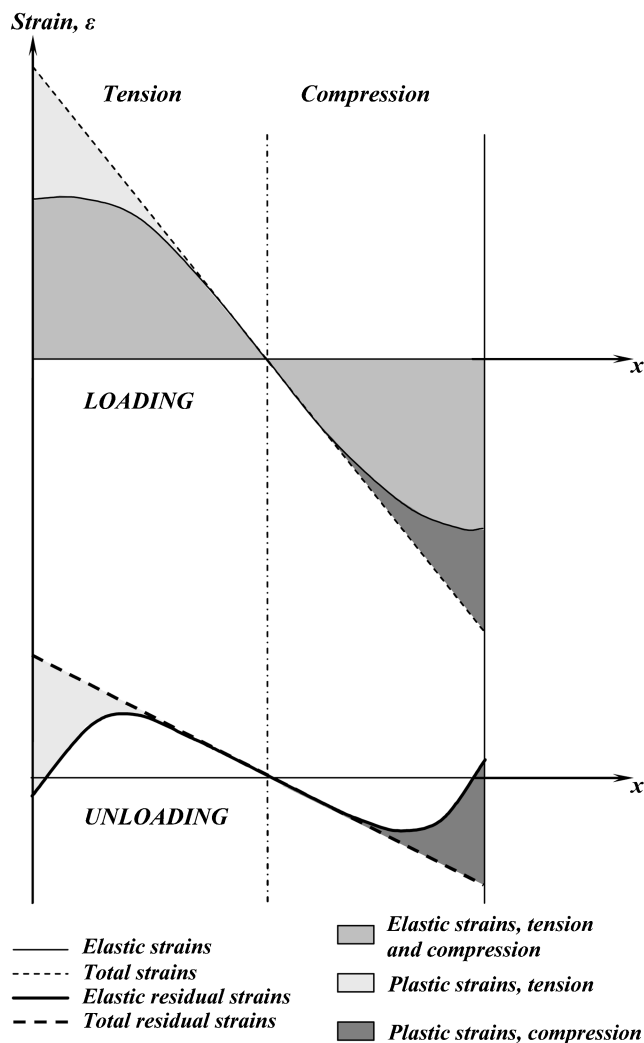


Fig. 3 Illustration of inelastic bending of a beam made from a work-hardening material (schematic)

portionality. The case when the applied moment exceeds the critical value is considered. The total strain still varies linearly across the beam, and is composed of the elastic strain given by the uniaxial tensile or compressive hardening curve, while the remaining strain is accommodated plastically. Elastic unloading is equivalent to the subtraction of a linear elastic strain profile, so the total residual strain profile is also given by the straight line (dashed), while the residual elastic strain is given by the S-shaped solid curve. The residual strain profile is symmetric if the material response to plastic deformation in tension and compression is also symmetric. The key property of the residual stress profile is that it must be self-equilibrating: the resultant force and moment across the bar must vanish.

The sample was mounted on the Euler cradle on station 16.3 at the synchrotron radiation source at Daresbury Laboratory. Apart from providing the usual rotational degrees of freedom (ω , χ , ϕ), the cradle is equipped with two translators allowing movement in the plane of the sample support platform. The photon energy used in the experiment was set to 50 keV. The incident beam spot size of $0.9 \text{ mm}^2 = 0.3 \text{ mm} \times 3 \text{ mm}$ was selected by a pair of horizontal and vertical motorized slits.

2.1 Monochromatic method: image plate

The recording of the diffraction peaks on to the phosphor plate is an extension of the Debye–Scherrer powder method. This method is widely employed to determine the crystal structures of polycrystalline components, namely to measure the scattering angles for a monochromatic X-ray beam directed at a polycrystalline material specimen. Owing to the polycrystallinity of the material, the X-ray scatter from a specific set of crystal planes with Miller indices, hkl , to form a cone with half-angle 2θ , where θ is related to the wavelength of the incident beam λ and the interplanar lattice spacing d , using Bragg's law

$$n\lambda = 2d \sin \theta \quad (1)$$

A recording of a plane section of the cone is made on photographic paper positioned a certain distance away from the specimen, resulting in a circle referred to as a powder circle, illustrated in Fig. 4.

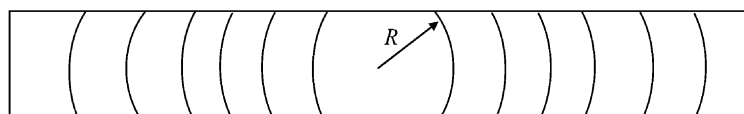


Fig. 4 Illustration of a recording of the powder circles on a strip of photographic paper

In a standard powder experiment the incident beam is directed at any part of the powder specimen, and the data are collected with the purpose of calculating crystal parameters. If, on the other hand, the beam is scanned across a powder-like sample (a polycrystal) that contains a variation in composition or lattice spacing (residual elastic strain), then the pattern of Debye–Scherrer circles shown in Fig. 5(a) would change with each scan step from point to point. In order to resolve these changes the sheet of photographic paper may be translated at the same time. If a narrow slit is used to restrict the width of the pattern on the recording medium, then only short segments of circles would be recorded on the photographic plate at each sample position, as shown in Fig. 5(b). There is an interest in establishing whether the same information can be extracted from the recording in terms of crystal plane orientation and diffraction strain as in the white beam data collection method.

A schematic of the set-up used to collect the diffraction peak data on the phosphoric plate from the bent magnesium alloy bar is shown in Fig. 6(a). The illustration shows the magnesium alloy specimen mounted on the table travelling at right angles to a stationary monochromatic X-ray beam. The IP was placed at a distance $L = 1495$ mm from the sample, as shown in Fig. 6(a). It was mounted on a translation table also capable of travelling across the incident X-ray beam. For the purposes of ease of set-up, the direction of travel of the IP was opposite to that of the specimen, although this choice of direction has no significance. The arrangement allowed the recording of a set of multiple powder circles arising from the monochromatic X-ray beam scattered from different points in the specimen translated perpendicular to the beam. A 3 mm-wide collimating lead slit was placed between the specimen and the IP in line with the incident beam. As a result a sequence of

narrow sections of powder circles was recorded. The position of each powder circle is identified with a diffraction angle 2θ , as shown in Fig. 7, which can be calculated from the known linear position of the corresponding peak on the IP using the known dimensions L and H , as shown in Fig. 8.

Figure 7 shows a typical image obtained during the recording of the powder circle segments while translating the IP simultaneously with the bent rectangular bar of magnesium alloy across the monochromatic beam [see Fig. 6(a)].

2.2 White beam method

The white beam ED set-up [1] was also used to collect data series of diffraction patterns from the sample. The station insertion device, the 6 T superconducting wavelength shifter, produces a smooth white beam spectrum with usable photons having energies up to 100 keV. Only photons with energies exceeding 50 keV were useful in the present experiment. The diffraction spectrum was recorded using a liquid cooled Ge detector (Canberra Model 8706 ADC). A multichannel analyser was used to bin the pulses from the amplifier.

The sample was mounted as shown in Fig. 6(b). The translation x axis perpendicular to the incident beam direction was located on the stage attached to the Euler cradle. A slit aperture of 3 mm (horizontal) and 0.1 mm (vertical) for the incident beam were used in the experiment, and a 0.1 mm aperture (vertical) was also used for the diffracted beam. The z axis of the sample was designated as the z axis, and the third y axis was normal to both the x and z directions and formed a right-handed coordinate system.

Detector calibration was carried out using the procedure described by Liu *et al.* [4], firstly using a radioactive source and then using the diffraction

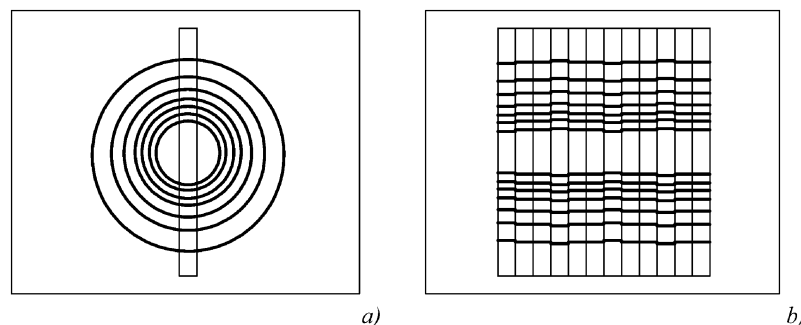


Fig. 5 Schematic of a recording of (a) a system of powder circles and (b) a sequence of powder circle segments recorded as the photographic plate is scanned in register with the polycrystalline specimen being translated across the monochromatic beam

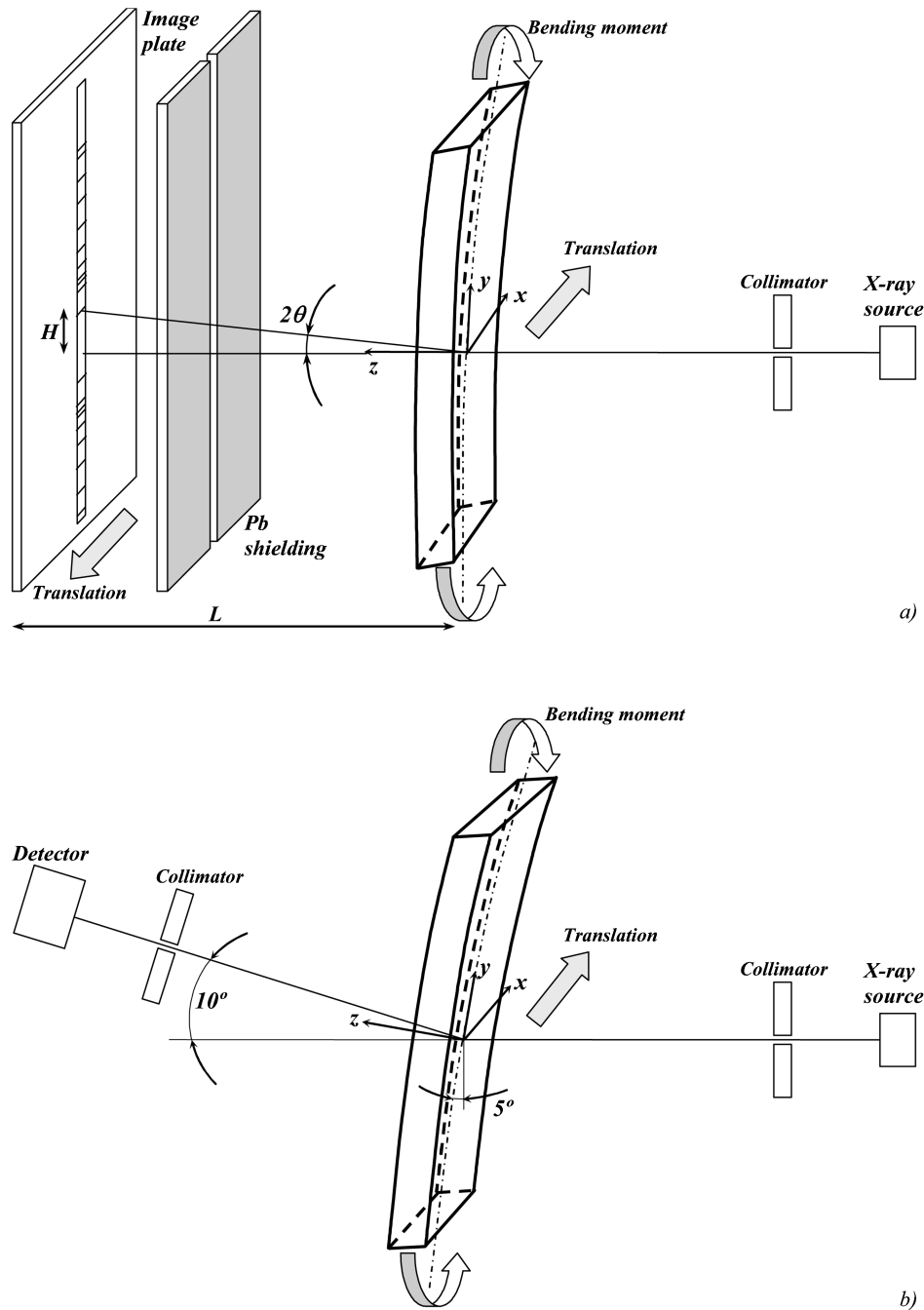


Fig. 6 Experimental set-ups (a) for the phosphor image plate measurement and (b) for the white beam mode measurement

pattern collected from the standard National Institute of Standards and Technology (NIST) silicon powder sample. The procedure involves careful step-wise calibration of the detector characteristic, with progressive improvement of the fit quality. Initial detector calibration was done using an Am^{241} radioactive source with an Mo filter. This provides photon flux at three distinct energies, although two of these energies are relatively close to each other, approxi-

mately at 15, 20, and 60 keV. This is insufficient to determine the non-linear detector characteristic, but allows approximate linear calibration. At the next stage a diffraction pattern is collected from a powder of a standard material (e.g. NIST Si) with a precisely known lattice structure and parameters. Starting with the previously known linear detector calibration, the quadratic characteristic of the detector is sought by requiring the best fit to the diffraction pattern. It is

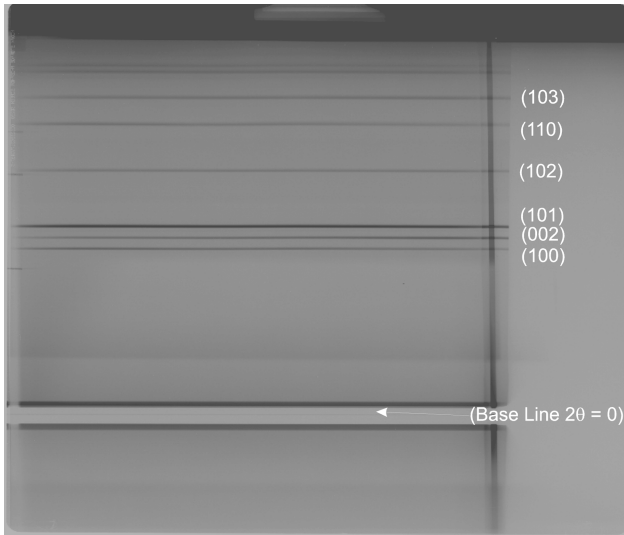


Fig. 7 Phosphor image plate recording showing the lines that correspond to the scattered powder circle segments

important to note, in passing, that if the diffraction angle is not known precisely, it can be determined at this stage together with the channel-to-energy conversion.

3 ANALYSIS

The residual strain profile can be obtained from the diffraction data by differentiating equation (1) as shown below

$$\frac{\Delta d}{d} = -\cot \theta \Delta \theta \quad (2)$$

In the ED set-up the right-hand side of equation (2) remains fixed. It can therefore be shown from simple analysis that

$$\frac{\Delta d}{d} = -\frac{\Delta E_\lambda}{E_\lambda} \quad (3)$$

The strain may therefore readily be found by

$$\varepsilon = \frac{d - d_0}{d_0} = \frac{\Delta d}{d_0} \quad (4)$$

where d_0 denotes the unstrained lattice spacing.

3.1 Image plate

The analysis of the diffraction peak data captured on the A3 image plate was performed using a Matlab™ subroutine for data extraction of the two-dimensional X-ray pattern. Figure 9 shows a pseudo-three-dimensional representation of the scattered X-ray data contained in a subsection of the phosphor plate image. The strain profile in a specimen is calculated by monitoring the relative deviation of a typical 'ridge' visible in Fig. 9 from its reference position. It should be noted that the colour in this figure has no other physical meaning than the intensity of the diffracted peaks at each scanning position.

For clarity, a one-dimensional plot of a single line, or vertical section, through the IP image shown in Fig. 7 is shown in Fig. 10 in which the grey scale intensity is plotted as a function of position within the plate measured from its bottom edge vertically upwards. The position of the baseline (where $2\theta = 0^\circ$) and diffraction peak indices are indicated in Figs 7, 9, and 10. The strain profile across the width of the

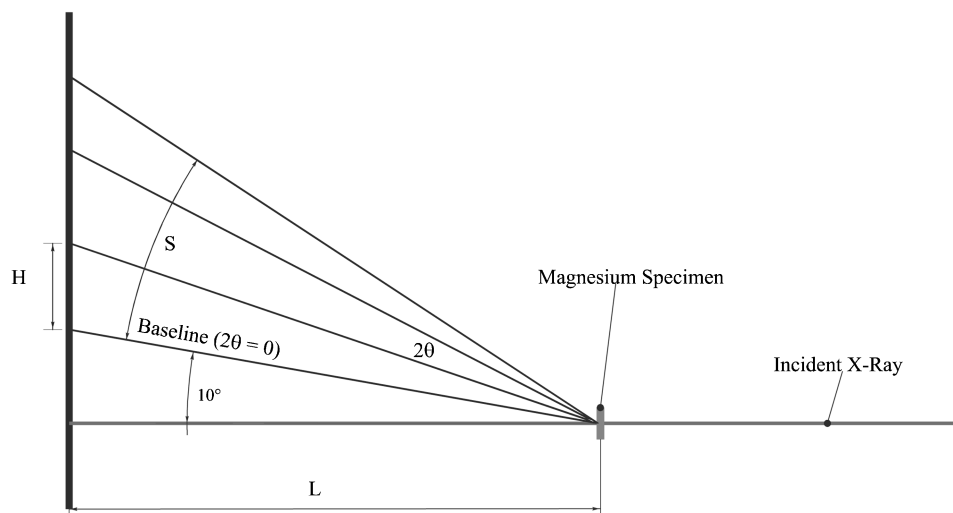


Fig. 8 Relation between the distance of the image from the specimen and the scattering angle 2θ

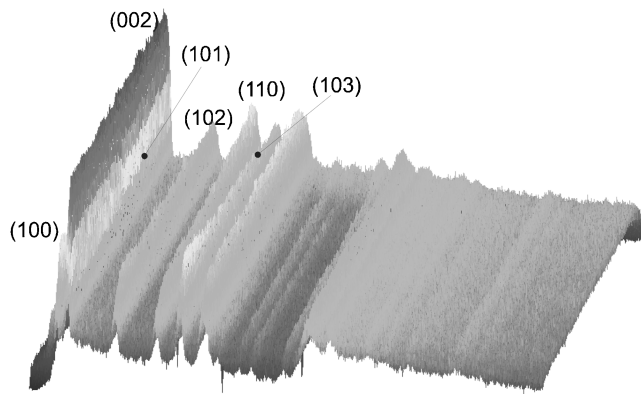


Fig. 9 A pseudo-three-dimensional representation of the data recorded on the image plate showing the evolution of peaks that correspond to specific types of crystal plane

magnesium alloy bar was obtained by monitoring the deviation of the centre of a particular peak from its reference position for each of the several families of crystal planes indicated in Fig. 10 [2]. Once the Miller indices of a particular set of crystal planes was specified, a MatlabTM single-peak fitting routine was employed to determine the peak centre position. Figure 11 shows a least-squares Gaussian fit in the form

$$f(x) = A_1 + A_2 e^{-[(x - A_3)^2 / (2A_4^2)]} \quad (5)$$

to one of the peaks corresponding to the 10.1 reflection.

In the process of data capture using the preliminary IP set-up, certain distortions and errors appeared in the profile. These effects are discussed and some rational procedures are offered for accounting and compensating for these distortions.

Although it was otherwise assumed during the set-up, rotation of the IP owing to the torsion and bending of the cantilever support of the IP translator contributed to apparent peak displacement of the diffracted X-ray beam. With lattice strains of the order of 10^{-4} or lower, even small deflections of the IP support system may be interpreted as strain. This was indeed the case in this set-up, but the associated effects on the data recorded by the IP were compensated for.

A peak correction function was therefore applied to the data extracted from the IP. The correction function was deduced by assuming that the error in the strain measurements arose primarily owing to two factors: (a) the bending of the IP support rail as the plate travels transversely to the incident X-ray beam and (b) the accompanying rotation of the IP around the incident beam. Figure 12 shows a schematic of the experimental set-up, illustrating the possible effects that lead to apparent variations in the strain.

The attenuated straight-through beam was also recorded on the IP and produced a baseline trace ($2\theta = 0^\circ$). This allowed the correction function to be calculated by evaluating the deviation of the baseline from a reference value. Figure 13 shows the peak

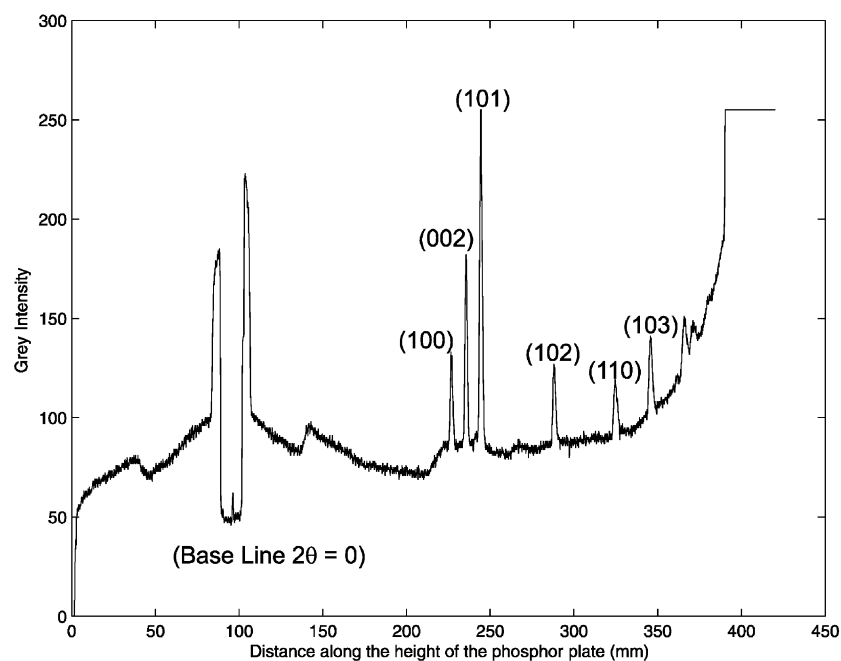


Fig. 10 Plot of a line through the phosphor plate showing the intensity as a function of the position on the plate measured in the direction of increasing 2θ . Peaks corresponding to different sets of crystal planes are indicated on the plot

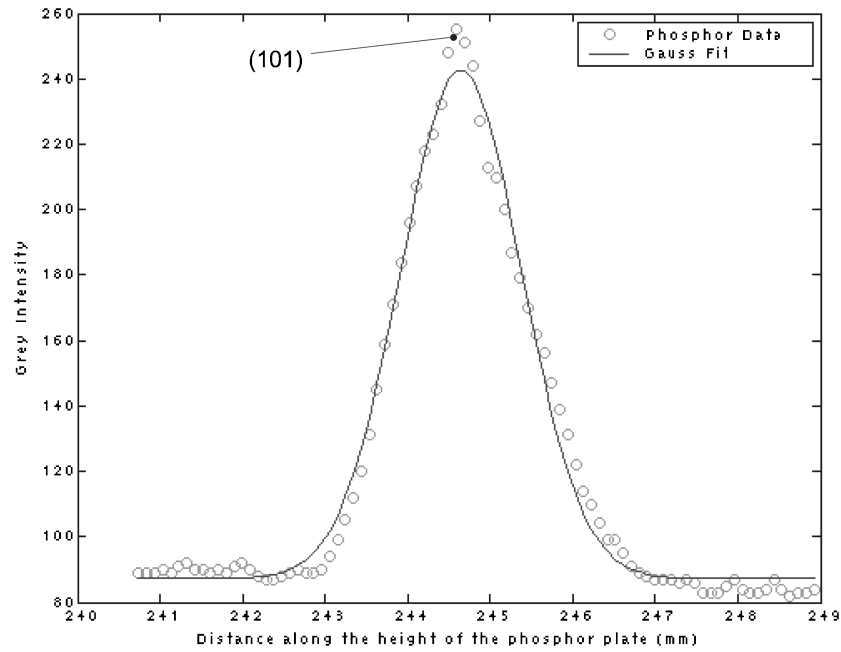


Fig. 11 Figure showing a Gaussian fit of the 101 plane as recorded on the phosphor plate at a particular position in the magnesium alloy specimen

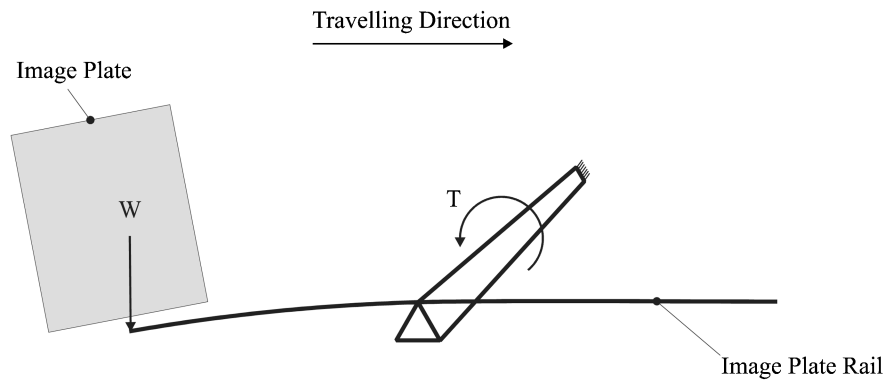


Fig. 12 A schematic illustration of the deflection effects in the experimental set-up that contribute to spurious apparent effects in the image plate data

correction function calculated using this method. Figure 14 shows the same function after correcting it to compensate for the rotational error induced during the scanning of the plate to extract the X-ray image. Also shown in this figure is the calculated deflection that resulted from the bending of the IP support rail.

In order to improve the confidence in the pattern correction procedure, the support rail deflection was also calculated analytically by assuming that the weight of the IP results in a concentrated force W acting through the IP's centroid at its instantaneous position. From simple beam theory the beam deflection equation is given by

$$\frac{d^2y}{dx^2} = -\frac{M_z}{EI_{xx}} \quad (6)$$

The deflection δ of a simple beam (such as the one under consideration) with a point load at its end can be written as

$$\delta = \frac{W}{6EI_{xx}}(2L^3 - 3Lx^2 + x^3) \quad (7)$$

where δ is measured positively in the direction of the deflection. E in this equation is Young's modulus to the beam, I_{xx} the second moment of area, L the beam's length, and x the distance measured from the beam's free end to the position through which W acts.

In practice the IP, or the force W in the schematic representing it, translated continuously along the beam during the experiment. Additional contributions to the deflection could have arisen from small deviations of the initial rail position from the

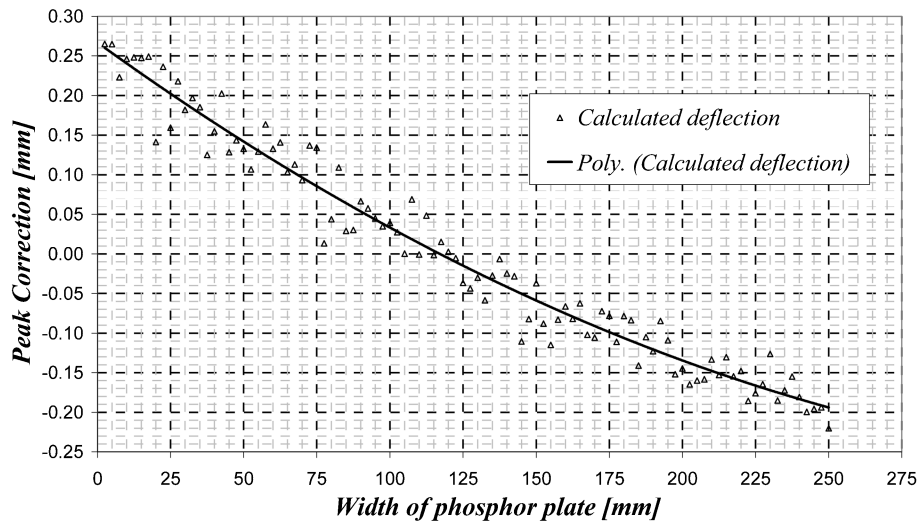


Fig. 13 Plot of the deviation of the reference straight-through beam position (baseline)

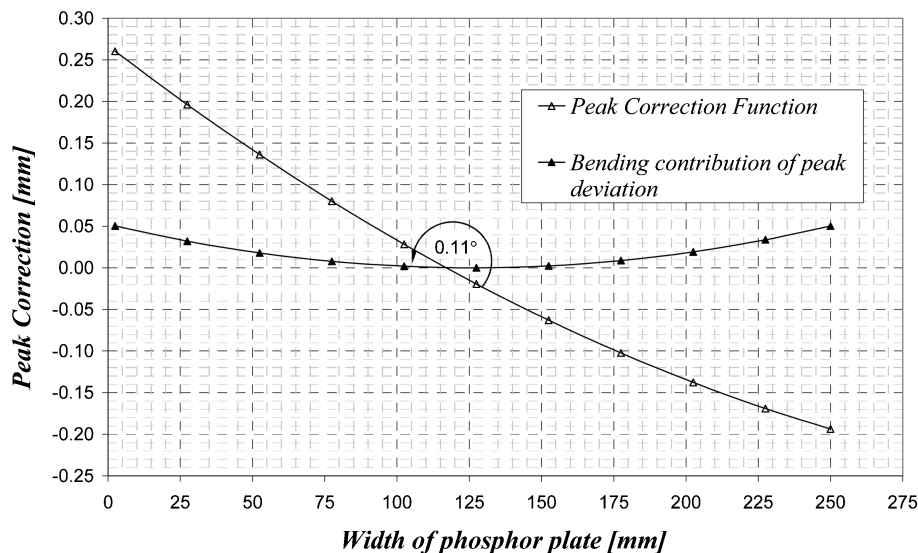


Fig. 14 Plot of the rotation correction function reflecting the contribution made by rail bending to apparent peak displacement

horizontal, etc. It is apparent from the form of equation (7), however, that a third-order polynomial should provide sufficient flexibility to provide a good approximation to the correction function for the IP data, allowing for the deflection resulting from bending. From the analysis it was found that the maximum deflection of the rail was of the order of 0.05 mm (50 μ m), while the maximum rotation of the IP during the scan amounted to 0.11°.

3.2 White beam

The analysis of the white beam diffraction patterns was carried out using the Rietveld refinement [3] adjusted for application to synchrotron ED data

[1, 4, 5] using the general structure analysis system (GSAS) [10]. In the white beam scan across the magnesium alloy bar, 60 individual measurements were collected. A typical pattern was selected for initial refinement using the GSAS, and the remaining data points are interpreted using a batch analysis subroutine written in Matlab™. The Matlab™ subroutine uses the variables from the initial refinement and calls the GSAS repeatedly to perform lattice parameter refinement and store the results in an output file.

The alloy studied in the present project had a single dominant phase (>90 per cent) with a hexagonal close-packed structure. Refinement was therefore performed using a single-phase crystal structure

model with the following parameters: space group P63/mmc, $a = 3.2094 \text{ \AA}$, and $c = 5.2108 \text{ \AA}$. The parameters that were refined included the background parameters, the coefficients for the ED peak profile function, and the two lattice parameters.

The profile obtained from X-ray ED experiments are dominated by electronic broadening in the detector system. This broadening is Gaussian and is assumed to be given by the function

$$f(\Gamma) = \frac{1}{\sqrt{2\pi}\eta^2} \exp\left(-\frac{\Gamma^2}{2\eta^2}\right) \quad (8)$$

where η is assumed to be a Gaussian broadening function expressed as a simple polynomial in terms of the X-ray photon energy E_λ as $\eta(E_\lambda) = \sqrt{A_1 E_\lambda^2 + A_2 E_\lambda + A_3}$. Γ is the reflection position taking into account the influence of deviatoric stresses and is expressed as

$$\Gamma = (E_\lambda - E_{\text{ph}}) - A_4 d \cos \gamma + A_5 \frac{(hk)^2 + (hl)^2 + (kl)^2}{h^2 + k^2 + l^2} \quad (9)$$

in which E_{ph} is the product of the various geometric and other correction factors for that reflection. For most crystal symmetries, γ is the angle between h and the n th-order major rotation axis of the space group. A_1 , A_2 , A_3 , A_4 , and A_5 are the five coefficients to be refined during the analysis.

The quality of a structural analysis is characterized by the residual R as

$$R_p = \frac{\sum |I_o - I_c|}{\sum I_o} \quad (10)$$

and

$$R_{\text{wp}} = \sqrt{\frac{\sum w(I_o - I_c)^2}{\sum w I_o^2}} \quad (11)$$

where I_o and I_c are the observed and calculated intensities respectively. The weighting factor w is given by $w = 1/\sigma^2$, where σ is the estimated statistical error for the intensity. The resulting observed and calculated diffraction patterns of the initial refinement are shown in Fig. 15. The refinement results are summarized in Table 2. The low values of R show satisfactory agreement between the experimentally observed and calculated diffraction patterns.

Table 2 Refinement results

Space group	P63/mmc
A	3.183122 \AA
C	5.174272 \AA
R_p	11%
R_{wp}	8%

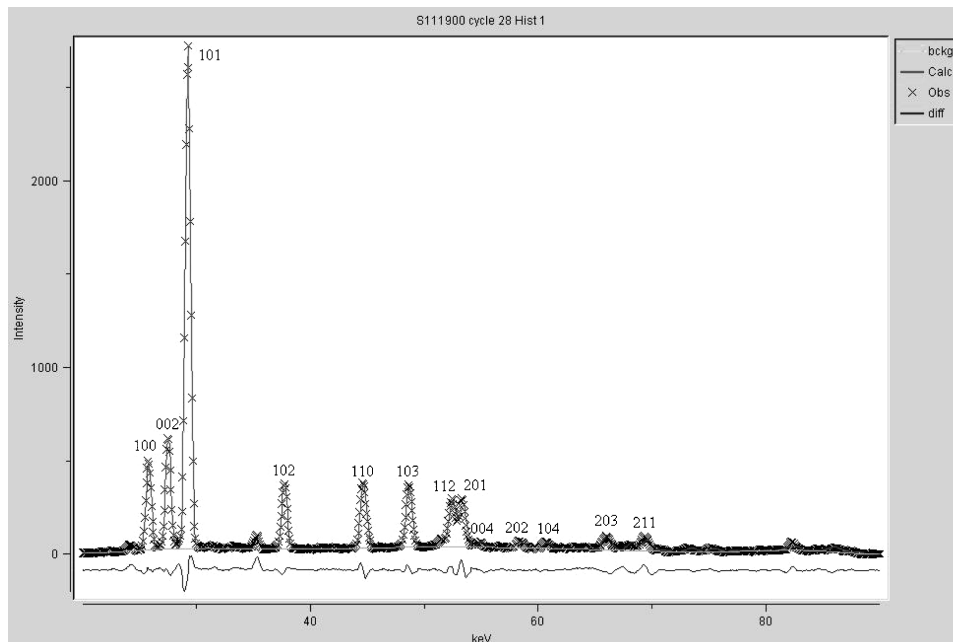


Fig. 15 Synchrotron diffraction data and the Pawley refinement of the diffraction pattern obtained from the magnesium alloy bar: the markers represent the observed data, while the continuous line represents the calculated profile; the difference curve at the bottom is drawn using the same scale

4 RESULTS AND DISCUSSION

The measurements obtained using the techniques described in the previous sections were analysed in order to find the residual elastic strains in the plastically bent magnesium alloy bar. The technique for white beam analysis has been studied and validated previously [1, 4] and has become largely standard [5]. Although the IP scanning technique has been used previously [11, 12], the authors are not aware of the image distortion corrections being applied to the data, or of attempts to perform whole pattern refinement on the patterns. In the present study, for the purposes of analysis, the two-dimensional image was broken into a number of strips of correct inclination (see the previous section)

that were extracted from the digitized image and converted into an effective one-dimensional profile. Each of the resulting line profiles was analysed using a MatlabTM routine to determine the displacement of peak centre positions. A series of files were also generated for input into the GSAS refinement program.

Figure 16 shows the comparison between residual elastic strain profiles calculated for the diffraction peaks 10.0 and 00.2 using the translating image plate and white beam modes. The differences should be noted between the two sets of results displayed using hollow circle markers (white beam mode) and solid triangle markers (translating image plate mode). While there is a clear qualitative agreement between the two sets of results, a quantitative comparison reveals that

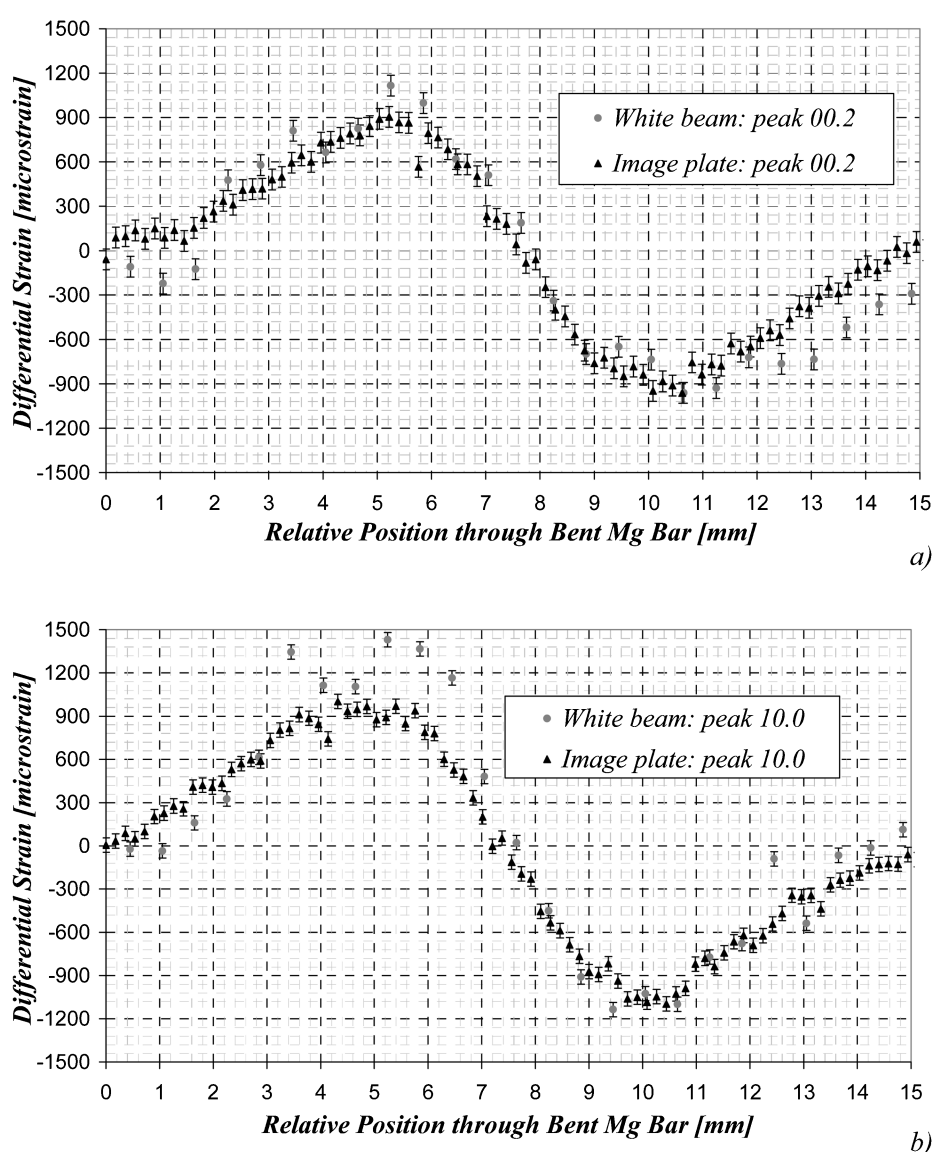


Fig. 16 Comparison between residual elastic strain profile calculated diffraction peaks (a) 00.2 and (b) 10.0, collected using the translating image plate and white beam modes

differences of up to about 300–400 microstrains are observed in the strain profiles. As a rule of thumb, the corresponding stress evaluation error amounts to about 25 MPa. In comparison, the full range of nominal residual stress computed on the basis of the strain profiles shown corresponds to about 150 MPa. It should also be noted that the IP data appear to be significantly smoother and less prone to scatter than the white beam measurements.

The origin of the difference between the two sets of results lies in the nature of the two experimental techniques employed. Firstly, the spatial resolution (in terms of beam width) of the ED measurements was considerably lower (about 0.5 mm) than that of

the IP measurements (about 0.2 mm). On the other hand, the IP data were collected in a continuous translating mode, thus ensuring that some continuous running average was obtained as a result. This guarantees that, even for relatively coarse-grained materials such as that of the present sample, the effect of individual grain orientation and deformation state on the computed strain values is minimized, and a smooth profile is produced. In fact, a similar effect could be achieved for the ED measurement mode, and would provide a better basis for comparison, but this was not attempted in the present study.

The difference in sign between the IP and ED results is observed at the front surface (near position

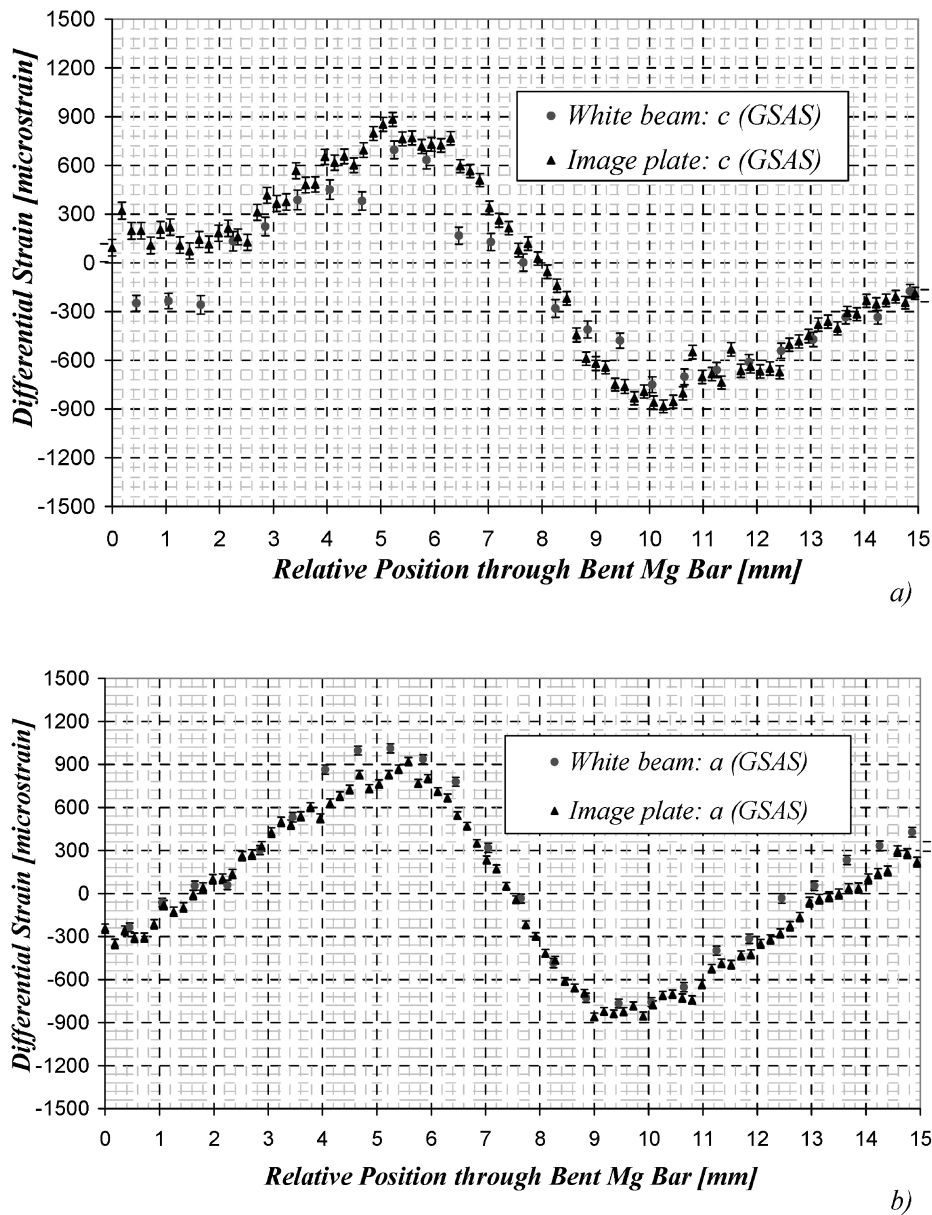


Fig. 17 Comparison of the strain profiles calculated on the basis of (a) *c* and (b) *a* parameters of the hcp lattice using an image plate and the white beam set-up

0 mm) in the 00.2 strain profile. This difference in itself is not significant, since the strain values are computed on the basis of a 'strain-free' lattice parameter value, so that only the absolute difference between the strain values (about 300 microstrains) is meaningful.

In principle, it is well known that the residual elastic strain profile must correspond to a self-equilibrating residual stress field, i.e. stress equilibrium and moment balance conditions for residual stress must be satisfied. However, imposing such a requirement depends on the knowledge of all the relevant strain components, so that longitudinal stress in the bar could be computed. In the present study only a single component of strain was measured, so that stress and moment balance conditions cannot be applied. An alternative approach to this problem would consist of seeking a distribution of permanent inelastic strain (eigenstrain) within the bar that would give rise (through the process of elastic equilibration) to the observed residual elastic strain profile(s). The advantage of the eigenstrain approach lies in the fact that the residual stress distribution then becomes a function of the putative eigenstrain distribution, and the requirements of stress and moment equilibrium are automatically enforced simultaneously with the requirement to provide the best match with the measured strain data [6].

The consideration of inelastic bending shows that the very central part of the beam remains elastic throughout the loading and unloading process. It is therefore readily possible to extract information about the plastic strain profile in the bent bar by subtracting the measured residual elastic strain curve from a straight line fitted to the central part of the profile. This operation can be performed for different reflections, thus allowing the plastic strain profiles to be obtained for groups of grains of different orientation. Figure 17 shows the comparison between the strains calculated on the basis of a and c lattice parameters using the IP mode and from the analysis of ED diffraction data using the GSAS. The agreement between the data obtained using these two modes is very good and shows that both are well suited for the purposes of polycrystalline deformation analysis in metallic alloys.

5 CONCLUSIONS

The residually bent bar of magnesium alloy considered in the present study provides a convenient test sample for establishing the comparative per-

formance of two methods aimed at fast collection of diffraction data, namely the monochromatic mode with translating IP and the white beam ED mode. The hcp (hexagonal close-packed) structure of the dominant phase in the magnesium alloy results in a large number of peaks available for fitting, providing excellent accuracy of lattice parameter determination.

Diffraction pattern refinement techniques were applied to both monochromatic IP and white beam ED data, but only after appropriate correction and calibration. It was shown that similar levels of accuracy in the determination of hcp lattice parameters a and c could be achieved using both methods. Furthermore, the mismatch in the strain response of different reflections could also be detected (difference strain) and correlated with plastic strain.

The translated IP technique is capable of providing a very good resolution and rate of data acquisition.

REFERENCES

- 1 Korsunsky, A. M., Collins, S. P., Owen, R. A., Daymond, M. R., Aichtioui, S., and James, K. E. Fast residual stress mapping using energy-dispersive synchrotron X-ray diffraction on station 16.3 at the SRS. *J. Synchrotron Radiation*, 2002, **9**(2), 77–81.
- 2 Korsunsky, A. M., Wells, K. E., and Withers, P. J. Mapping two-dimensional state of strain using synchrotron X-ray diffraction. *Scripta Materialia*, 1998, **39**(12), 1705–1712.
- 3 Rietveld, H. A profile refinement method for nuclear and magnetic structures. *J. Appl. Crystallography*, 1969, **2**(2), 65–71.
- 4 Liu, J., Kim, K., Golshan, M., Laundy, D., and Korsunsky, A. M. Energy calibration and full-pattern refinement for strain analysis using energy-dispersive and monochromatic X-ray diffraction. *J. Appl. Crystallography*, 2005, **38**(4), 661–667.
- 5 Steuwer, A., Santisteban, J. R., Turski, M., Withers, P. J., and Buslaps, T. High-resolution strain mapping in bulk samples using full-profile analysis of energy-dispersive synchrotron X-ray diffraction data. *J. Appl. Crystallography*, 2004, **37**(6), 883–889.
- 6 Korsunsky, A. M., Daymond, M. R., and James, K. E. The correlation between plastic strain and anisotropy strain in aluminium alloy polycrystals. *Mater. Sci. Engng A*, 2002, **334**(1–2), 41–48.
- 7 Kouadri, A. and Barrallier, L. Texture characterisation of hexagonal metals: magnesium AZ91 alloy, welded by laser processing. *Mater. Sci. Engng A*, 2006, **429**(1–2), 11–17.
- 8 Parco, M., Zhao, L., Zwick, J., Bobzin, K., and Lugscheider, E. Investigation of HVOF spraying on magnesium alloys. *Surface and Coatings Technol.* (in press).

- 9 Golshan, M., Liu, J., Kim, K., Laundry, D., Dini, D., and Korsunsky, A. M. Analysis of plastic deformation and residual elastic strain in a titanium alloy using synchrotron X-ray diffraction. *J. Physics D: Appl. Physics*, 2005, **38**(10A), A195.
- 10 Larson, A. C. and Von Dreele, R. B. General structure analysis system (GSAS). Los Alamos National Laboratory Report LAUR, 2000.
- 11 Kinne, A., Thoms, M., Röss, H. R., Gerhard, T., Ehinger, M., Faschinger, W., *et al.* Image plates as one-dimensional detectors in high-resolution X-ray diffraction. *J. Appl. Crystallography*, 1998, **31**(3), 446–452.
- 12 Thoms, M., von Seggern, H., and Winnacker, A. Spatial correlation and photostimulability of defect centers in the X-ray-storage phosphor BaFBr-Eu²⁺. *Phys. Rev. B*, 1991, **44**(17), 9240LP–9247.

APPENDIX

Notation

d	interplanar spacing of polycrystalline material (Å)	E_λ	X-ray photon energy (keV)
d_0	unstrained lattice spacing (Å)	H	height of the diffraction peak from the datum Bragg angle (m)
E	Young's modulus (Pa)	I_c	calculated intensity
E_{ph}	correction factor	I_o	observed intensity
		I_{xx}	second moment of the area (m ⁴)
		L	distance of the specimen to the phosphoric plate (m)
		M_z	bending moment about the z axis (N m)
		n	diffraction order
		R	goodness of least-squares GSAS fit to the multiple peak spectrum
		w	least-squares weight
		W	load (N)
		γ	angle between h and the n th-order rotation angle (deg)
		Γ	reflection position (keV)
		δ	deflection (m)
		ε	strain (m/m)
		θ	Bragg angle (deg)
		λ	X-ray photon wavelength (Å)
		σ	estimated statistical error
		ϕ	rotational degree of freedom (deg)
		χ	rotational degree of freedom (deg)
		ω	rotational degree of freedom (deg)